

SUPPLEMENTARY INFORMATION

Incorporating Zeolitic-Imidazolate Framework-8 nanoparticles into kidney scaffolds: a first step towards innovative renal therapies

Fátima Guerrero,^{*a,b} Victoria Pulido,^{a,b} Said Hamad,^e Pedro Aljama,^{a,b} Alejandro Martín-Malo^{a,b,c,d} and Carolina Carrillo-Carrión^{*f,g}

^aMaimonides Biomedical Research Institute of Cordoba (IMIBIC), Reina Sofia University Hospital, 14004 Córdoba, Spain. Co-corresponding author (F.G.), Email: fatima.guerrero@imibic.org

^bDepartment of Medicine, University of Cordoba, 14004 Córdoba, Spain.

^cNephrology Unit, Reina Sofia University Hospital, 14004 Córdoba, Spain.

^dSpanish Renal Research Network, Institute of Health Carlos III, 28040 Madrid, Spain.

^eDepartment of Physical, Chemical and Natural Systems, University Pablo de Olavide, 41013 Seville, Spain.

^fInstitute for Chemical Research (IIQ), CSIC-University of Seville, 41092 Sevilla, Spain. Corresponding author (C.C.-C.), Email: carolina.carrillo@csic.es

^gDepartment of Organic Chemistry, Faculty of Chemistry, University of Seville, 41012 Seville, Spain.

TABLE OF CONTENTS

I. Synthesis of polymer-modified zeolitic-imidazolate framework-8 nanoparticles

I.1. Synthesis of ZIF-8 nanoparticles

I.2. Functionalization of ZIF-8 nanoparticles with PMA polymer (nanoZIF8@PMA)

I.3. Preparation of rhodamine-loaded nanoZIF8@PMA

I.4. Preparation of rhodamine-loaded nanoZIF8@PMA-fluoresceinamine

II. Morphological/Structural characterization

II.1. Scanning Electron Microscopy (SEM)

II.2. Powder X-Ray Diffraction (PXRD)

II.3. Dynamic Light Scattering (DLS) and Zeta-Potential (ζ)

II.4. ¹H Nuclear Magnetic Resonance (¹H NMR)

II.5. Thermogravimetric analysis (TGA)

II.6. N₂ Physisorption analysis

III. Adsorption experiments of toxins by nanoZIF8@PMA under static conditions

III.1. Procedure of adsorption experiments

III.2. Quantification of toxins by UV/Vis spectroscopy

III.3. Optimization of adsorption conditions

III.4. Crystallinity of particles after toxins adsorption

III.5. Data comparison with other MOFs reported

IV. Immobilization of nanoZIF8@PMA within a rat kidney scaffold

IV.1. Kidney decellularization protocol

IV.2. Perfusion of nanoparticles through a kidney scaffold

V. Performance evaluation of ZIF8-modified scaffold

V.1. Procedure of adsorption experiments under flow conditions

V.2. Quantification of toxins by RP-HPLC-DAD

V.3. Evaluation of the reusability of ZIF8-modified scaffold

V.4. Statistical analysis

VI. Computational study of the adsorption of toxins in ZIF-8

VI.1. Computational details

VI.2. Adsorption of pC and IS, pure and mixed with phosphate molecules

VII. References

I. Synthesis of polymer-modified zeolitic-imidazolate framework-8 nanoparticles

All the reagents including zinc nitrate hexahydrate ($\text{Zn}(\text{NO}_3)_2 \cdot 6\text{H}_2\text{O}$; Sigma Aldrich #96482), 2-methylimidazole (Melmz; Sigma Aldrich #M50850), hexadecyltrimethylammonium bromide (CTAB; Sigma Aldrich #H5882) and rhodamine B (RhB; Sigma Aldrich #R6626) were used as purchased without any purification. Poly[isobutylene–alt–maleic anhydride]–graft–dodecyl (PMA), an amphiphilic polymer, was synthesized according to a previously reported protocol.¹

I.1. Synthesis of ZIF-8 nanoparticles

The synthesis was carried following a previously reported protocol.² Briefly, 3 mL of Melmz (aqueous solution at 1.3 M) were placed in a 12-mL glass vial with a magnetic stir bar, followed by the addition of 3 mL of $\text{Zn}(\text{NO}_3)_2$ (aqueous solution at 0.025 M) under continuous gentle stirring and at room temperature (RT). Next, 3 mL of CTAB (aqueous solution at 1.1×10^{-3} M) were immediately added, the mixture was stirred for 2 min, and left then undisturbed at RT overnight (15 h). The mixture slowly turned turbid with white milky color, indicating the formation of the ZIF-8 nanoparticles. Next day, the particles were collected by centrifugation (7000 RCF, 5 min), washed three times with methanol, vacuum-drying at 60 °C and finally redispersed in methanol at a concentration of 10 mg·mL⁻¹.

I.2. Functionalization of ZIF-8 nanoparticles with PMA polymer (nanoZIF8@PMA)

To stabilize the ZIF-8 nanoparticles in aqueous solution and at the scaffold microenvironment, they were functionalized with an amphiphilic polymer (PMA) following a reported procedure,² but using a lower ratio (R) of monomers of PMA per nm² surface of ZIF-8 particle ($R = 100$) to avoid that an excess of polymer on the surface could block the entrance pores and limit the effective adsorption of toxins in the internal pores of the framework. Briefly, the ZIF-8 nanoparticles dispersed in methanol were mixed with 0.05 M PMA in chloroform solution, and the solvent (3:1 MeOH:CHCl₃) was slowly evaporated in a rotary evaporator. The dried product was then resuspended by adding *ca.* 5 mL of 0.1 M NaOH solution. The resulting particles were collected by centrifugation (7000 RCF, 10 min), washed twice with water, and finally redispersed in water at a concentration of 10 mg·mL⁻¹ (mass concentration calculated considering only the core ZIF-8 particles and not the polymer coating). The core size of the as-produced nanoZIF8@PMA particles as determined by SEM remained the same as the original ZIF-8 nanoparticles (~120 nm) but the corners become slightly rounded (Fig. S1).

I.3. Preparation of rhodamine-loaded nanoZIF8@PMA

To easily visualize the nanoZIF8@PMA particles within the renal scaffold, these particles were loaded with a fluorescent dye (rhodamine B, RhB) before their PMA functionalization. For that, the as-synthesized ZIF-8 nanoparticles as dispersed in methanol (0.2 mL, 10 mg·mL⁻¹) were mixed with a solution of RhB in MeOH (100 µL, 1 mg/mL), having thus 50 mg dye/g ZIF-8 during the incubation. The mixture was incubated overnight at RT to ensure that the maximum loading was reached. Then the excess of the dye was removed by centrifugation and the RhB-loaded ZIF8 particles were washed twice with MeOH in order to remove the RhB weakly adsorbed onto the ZIF-8 surface. The loading amount of RhB was calculated by subtracting the mass of RhB in the supernatants from the total mass of the dye in the first initial solution by UV-vis spectroscopy at 550 nm. Data revealed a high loading capacity for rhodamine (36.6 mg RhB per g ZIF-8

nanoparticles), which corresponds to a loading efficiency of 73 %. Next, these RhB-loaded ZIF8 particles were stabilized by functionalization with PMA polymer following the same procedure described in section 1.2, finally obtaining RhB-nanoZIF8@PMA particles. RhB-nanoZIF8 particles were used as a control to reveal the importance of PMA for the effective immobilization of the particles within the scaffold.

1.4. Preparation of rhodamine-loaded nanoZIF8@PMA-fluoresceinamine

For monitoring the potential degradation of the nanoZIF8@PMA during immobilization and/or possible detaching of the polymer during the perfusion of toxin solutions through the modified scaffold, PMA was labelled with a fluorescent dye (fluoresceinamine, FA). The modification of the polymer with the fluorophore molecules was performed according to previously reported optimized procedures.^{3,4} Briefly, a stock solution of FA (dissolved in methanol) was mixed with the PMA solution (dissolved in chloroform) in a ratio of 2 % (*i.e.* fluorophore/PMA monomer ratio of 2/100), and the mixture was stirred at RT overnight. Next day, organic solvents were evaporated using a rotavap, and the resulting powder was redissolved in chloroform to obtain a final (monomer) polymer concentration of 0.05 M. This PMA-FA polymer was used to functionalize the RhB-nanoZIF8 particles following the same procedure described in section 1.2, finally obtaining RhB-nanoZIF8@PMA-FA particles. These doubly labelled particles, in the ZIF8 core with RhB and in the polymer surface with FA, were used to study the stability or degradation of the particles during use by combining measurements of fluorescence of the perfused solution and confocal microscopy of kidney scaffold transverse sections.

II. Morphological/Structural characterization

II.1. Scanning Electron Microscopy (SEM)

SEM analysis was carried out to investigate the morphology (shape and size) of ZIF-8 nanoparticles before (nanoZIF8) and after the polymer functionalization (nanoZIF8@PMA). The analysis was performed in a JEOL JSM 7800F scanning electron microscope in backscattered electron mode at 3 kV. Samples were prepared by drying, under ambient conditions, a diluted dispersion of the particles on a silicon wafer substrate.

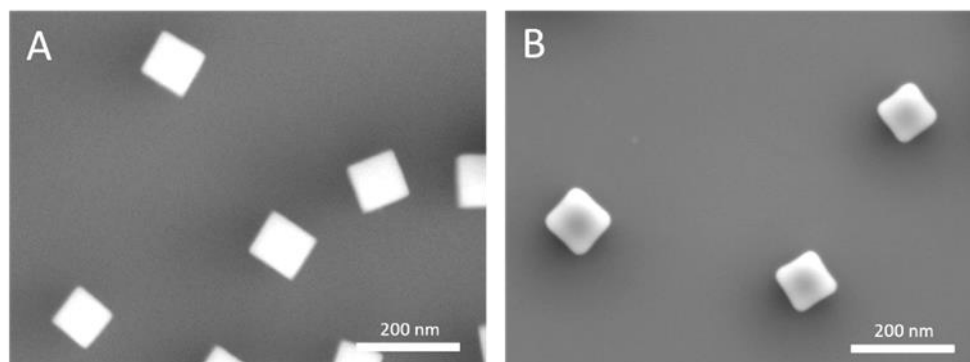


Fig. S1. Representative SEM images of (A) nanoZIF8, and (B) nanoZIF8@PMA particles.

II.2. Powder X-Ray Diffraction (PXRD)

X-ray analysis of the crystalline powder of samples was performed using a Bruker D8-Advance Diffractometer. X-ray radiation of Cu K α was used and the measurement range was from 3° to 70° (2 θ) with a step of 0.02° (2 θ). To check the stability of these particles in a phosphate saline buffer (PBS, 0.1 M, pH=7.4), the particles were incubated in PBS for 24 h, followed by centrifugation, washing once with methanol, and vacuum-drying at 60 °C; the PXRD of these samples after PBS treatment was also measured (Fig. S2). The obtained PXRD patterns could be indexed using a cubic system with space group I-43m demonstrating the typical sodalite (SOD) zeolite-type structure, and confirming ZIF-8 particles were successfully synthesized. Simple visual inspection of the patterns showed slight changes in the peak intensity of some peaks after PMA functionalization but the crystalline structure was preserved. Such observation may be attributed to changes in preferred orientation or texture, and/or the formation of some defects during the procedure of polymer modification. On the other hand, it was found that whereas nanosized ZIF-8 particles were not stable in PBS as previously reported, the polymer functionalization endowed the ZIF8 particles with structural stability in the presence of phosphate ions. Due to this lack of structural stability of nanoZIF8 particles in PBS, further experiments for colloidal stability over time in PBS and solutions of toxins in PBS were only carried out with stable nanoZIF8@PMA particles.

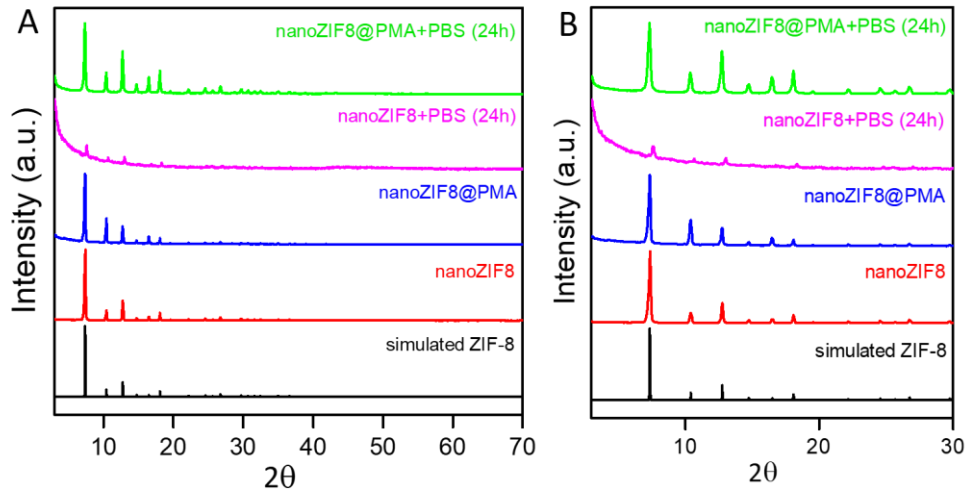


Fig. S2. PXRD patterns of nanoZIF8 and nanoZIF@PMA particles as-prepared and after incubation with PBS. For comparison, simulations of ZIF-8 (black, COD (Crystallography Open Database): 7111970) is added. (A) spectrum from 3° to 70° (2θ), and (B) magnification of the 2θ range between 3° and 30° to clearly visualize changes between samples.

II.3. Dynamic Light Scattering (DLS) and Zeta-Potential (ζ)

Measurements were performed using a Malvern Zetasizer Nano ZSP equipped with a 10 mW He–Ne laser operating at a wavelength of 633 nm and fixed scattering angle of 173°. DLS analysis was used to measure the hydrodynamic diameter (d_h) from the number distribution of the nanoZIF8@PMA particles dispersed in PBS (0.1 M, pH=7.4). In order to evaluate their colloidal stability in PBS as well as in the presence of uremic toxins (pC and IS at 0.3 mM in PBS), DLS measurements were performed at different time points (Table S1). Data revealed that particles were stable up to 5 days in both studied media. The zeta-potential of nanoZIF8@PMA particles as dispersed in PBS was measured with laser Doppler anemometry (LDA) by using the same Malvern Zetasizer Nano ZSP instrument. The nanoZIF8@PMA particles were negatively charged ($\zeta = -25.3 \pm 0.5$ mV) as it was expected due to the carboxyl groups of the PMA polymer.

Table S1. Hydrodynamic diameters d_h (mean value \pm SD) as derived from DLS measurements of the nanoZIF8@PMA particles dispersed in PSB or in a PBS solution containing the uremic toxins (pC and IS at 0.3 mM). SD values correspond to the standard deviation of the diameter mean value as obtained from several repetitions ($n=3$) of the measurement. The polydispersity index (PDI) for each sample is also given. Data correspond to raw data depicted in Fig. 1D.

| Time (h) | PBS | | Toxins solution | |
|----------|-------------|------|-----------------|------|
| | d_h (nm) | PDI | d_h (nm) | PDI |
| 0 | 128 \pm 4 | 0.11 | 132 \pm 7 | 0.19 |
| 24 | 122 \pm 6 | 0.17 | 138 \pm 4 | 0.18 |
| 48 | 120 \pm 7 | 0.15 | 141 \pm 9 | 0.17 |
| 72 | 117 \pm 8 | 0.17 | 144 \pm 9 | 0.19 |
| 96 | 123 \pm 8 | 0.22 | 137 \pm 8 | 0.20 |
| 120 | 125 \pm 9 | 0.21 | 135 \pm 10 | 0.23 |

II.4. ^1H Nuclear Magnetic Resonance (^1H NMR)

^1H NMR spectra were recorded at 25 °C in MeOD using a 400 MHz Bruker Avance III HD spectrometer. Chemical shifts are in ppm with respect to TMS (tetramethylsilane) using the manufacturer indirect referencing method. These ^1H NMR spectra (Fig. S3) confirmed that the ZIF-8 was successfully modified with the PMA polymer.

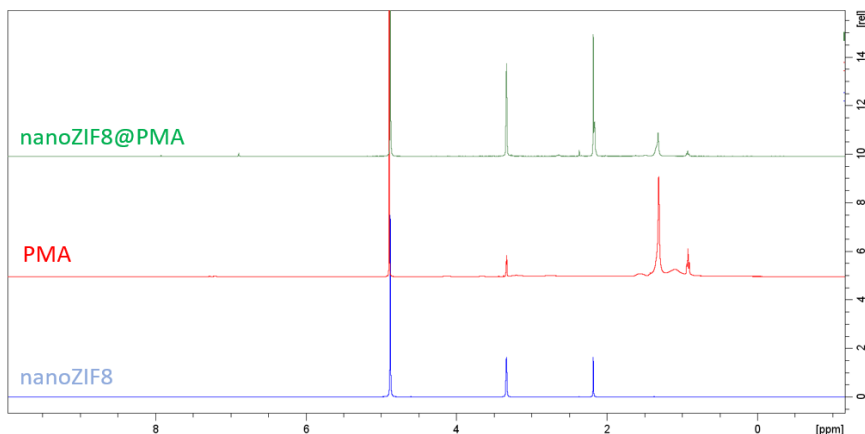


Fig. S3. ^1H -NMR spectra of nanoZIF8, PMA polymer, and nanoZIF@PMA particles as dispersed in MeOD. Note the peaks at 4.9 and 3.3 ppm arises from the solvent.

II.5. Thermogravimetric analysis (TGA)

To investigate the thermal behavior of the nanoparticles, thermogravimetric analysis (TGA) under air (Fig. S4) was performed using a Thermal Advantage SDT-600 instrument with a general heating profile from 30 to 700 °C and using a heating rate of 5 °C·min⁻¹ under air in a flow of 100 mL·min⁻¹. nanoZIF8 particles presented a sharp weight loss (50–60 wt%) at around 400 °C, consistent with the total combustion of 2-methylimidazole and the formation of inorganic ZnO residues. In contrast, nanoZIF8@PMA particles showed three mass loss steps: (1) an initial mass loss of ca. 4 wt% between 30–120 °C relative to the water content in the sample; (2) a second mass loss of ca. 36 wt% associated with the PMA glass transition within the range of 200–350 °C; and (3) a final mass loss of ca. 38 wt% at around 350–500 °C due to the combustion of 2-methylimidazole. These results are in accordance with previous studies. From these data the amount of PMA polymer in the nanoZIF8@PMA particles was determined to be 36 wt%.

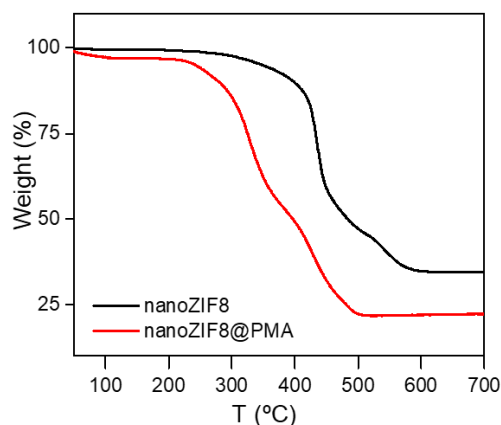


Fig. S4. TGA curves of nanoZIF8 and nanoZIF@PMA particles recorded in a dynamic air atmosphere.

II.6. N₂ Physisorption Analysis

N₂ sorption isotherm of nanoZIF8 and nanoZIF8@PMA particles was performed in an Autosorb-iQ-2 MP/XR (Quantachrome) at the liquid nitrogen temperature (77 K). The samples were degassed under high vacuum (overnight, 150 °C) before analysis. The specific surface areas were calculated from the Barrett–Emmett–Teller (BET) method in the pressure interval $P/P_0=0.01-0.3$ (being P_0 the saturation pressure). Pore volume and external surface area were calculated by the t-plot method. The N₂ isotherms of samples and the calculated textural properties are shown in Fig. S5 and Table S2, respectively. Taking into account that the PMA part in the nanoZIF8@PMA particles accounts for a 36 %wt as determined by TGA, their textural data were corrected considering exclusively the ZIF-8 weight.

Table S2. Textural properties of nanoZIF8 and nanoZIF8@PMA particles.

| Sample | S_{BET} ($\text{m}^2\cdot\text{g}^{-1}$) | V_{micro} ($\text{cm}^3\cdot\text{g}^{-1}$) | S_{BET} ($\text{m}^2\cdot\text{g}^{-1}$)* | V_{micro} ($\text{cm}^3\cdot\text{g}^{-1}$)* |
|--------------|--|---|---|--|
| nanoZIF8 | 1630 | 0.768 | - | - |
| nanoZIF8@PMA | 1143 | 0.505 | 1786 | 0.789 |

*corrected considering exclusively the ZIF-8 weight.

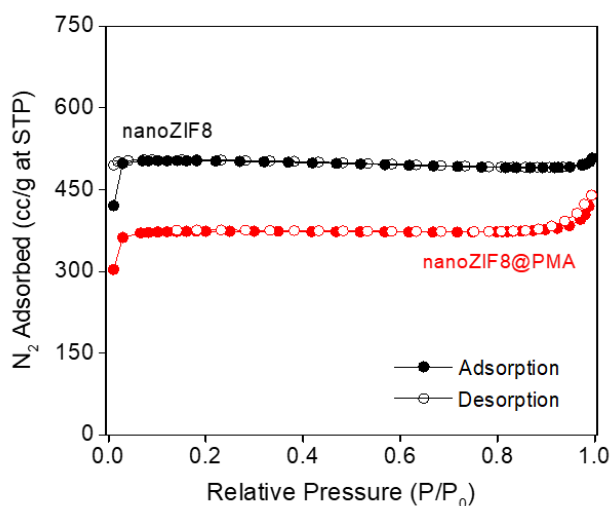


Fig. S5. Experimental N₂ adsorption and desorption isotherms for nanoZIF8 and nanoZIF8@PMA particles.

III. Adsorption experiments of toxins by nanoZIF8 under static conditions

PBS (0.01 M, pH=7.4) was prepared by dissolving PBS tablets (Sigma-Aldrich #P4417) in Milli-Q water. Uremic toxins, including indoxyl sulfate potassium salt (IS, Sigma-Aldrich #13875) and p-cresol (pC, Sigma-Aldrich #C85751), were used as purchased without any purification. Human serum (Sigma-Aldrich #H4522) was subjected to heat inactivation and filtered (0.2 μm filter) before use. A stock concentrated solution (0.1 M) of IS was prepared in water, and the working solutions were prepared by appropriate dilution of the stock solution with PBS or human serum. Similarly, a stock concentrated solution (0.1 M) of pC was prepared in methanol, and the working solutions were prepared by appropriate dilution of the stock solution. The working concentrations of pC and IS were set at 0.3 mM, based on mean concentrations found in CKD patients.^[5] Accordingly, 0.3 mM (75.4 $\mu\text{g}\cdot\text{mL}^{-1}$) of IS and 0.3 mM (32.4 $\mu\text{g}\cdot\text{mL}^{-1}$) of pC solutions in PBS were freshly prepared before use.

III.1. Procedure of adsorption experiments

In a typical experiment, nanoZIF8@PMA particles were added to in 5 mL of 0.3 mM pC or IS solution in a 10-mL glass vial, and the mixture was incubated under static conditions under specific conditions of time and temperature. After incubation, the nanoZIF8 particles were separated by centrifugation (7000 RCF, 10 min), and the amount of toxins (pC or IS) adsorbed on the nanoZIF8 was quantified by UV-Vis spectroscopy indirectly, by measuring the toxins remaining in the supernatants after centrifugation of the particles.

III.2. Quantification of toxins by UV/Vis spectroscopy

The toxin concentration in the supernatant was determined by interpolation of the measured absorbance (A) at the maximum absorption peak to a previously constructed analytical calibration curve (Fig. S6). The removal efficiency was calculated using the following Equation 1:

$$\text{Removal (\%)} = \frac{C_i - C_f}{C_i} \times 100 \quad \text{Equation 1}$$

where C_i = the initial concentration and C_f = the final concentration.

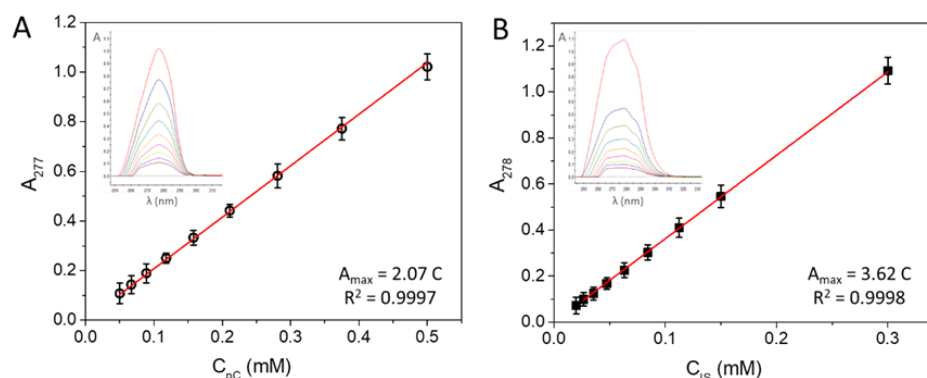


Fig. S6. Calibration curves of (A) pC and (B) IS in PBS medium as obtained from UV-Vis measurements of standard solutions. Insets show the UV-Vis spectra of the different standards. Absorbance (A) at the maximum absorption peak as a function of toxin concentration (c) is plotted and calibration equation is obtained by fitting a linear regression line to the collected data; R^2 is the coefficient of determination.

III.3. Optimization of adsorption conditions

In order to investigate the adsorption process of both toxins (pC and IS) on the nanoZIF@PMA the following parameters were studied: 1) amount of nanoZIF8@PMA (in the range from 5 to 20 mg), 2) temperature (37 °C versus RT), and 3) kinetics (removal efficiency over time). Regarding the particles' amount, the removal efficiency increased when increasing the mg of nanoZIF8@PMA, but the maximum toxins uptake capacity was reached for 10 mg (Fig. S7); the fact that larger quantities do not lead to higher absorption capacities could be attributed to aggregation issues or low dispersion of particles at such concentrated solution and under static conditions. On the other hand, the adsorption was enhanced at 37 °C compared to RT, as it was expected since temperature enhances mass transfer and diffusion in the micropores of the MOF. Kinetics studies revealed rather fast adsorption rates for both toxins, being pC adsorbed slightly faster due to their hydrophobic character and therefore better interaction with the hydrophobic pores and channels of ZIF-8.

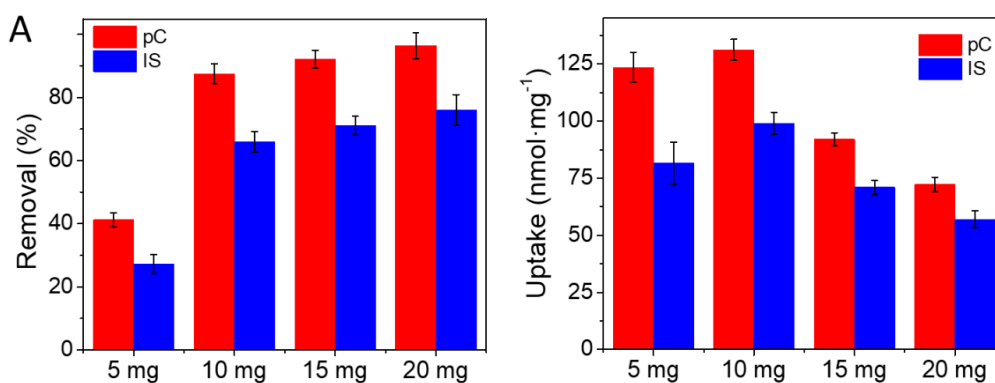


Fig. S7. (A) Removal efficiency and (B) uptake capacity of nanoZIF8@PMA particles towards pC and IS (0.3 mM in PBS) after 24 h incubation at 37 °C as a function of the number of particles (mg of particles).

III.4. Crystallinity of particles after toxins adsorption

To investigate if the crystalline nature of the nanoZIF8@PMA was affected after the adsorption of toxins, particles were incubated with the toxin solutions in PBS for 24 h at 37 °C, followed by centrifugation to separate particles, washing once with methanol, and vacuum-drying at 60 °C. PXRD experiments confirmed that the crystalline structure of the particles was preserved after the toxin adsorption (Fig. S8).

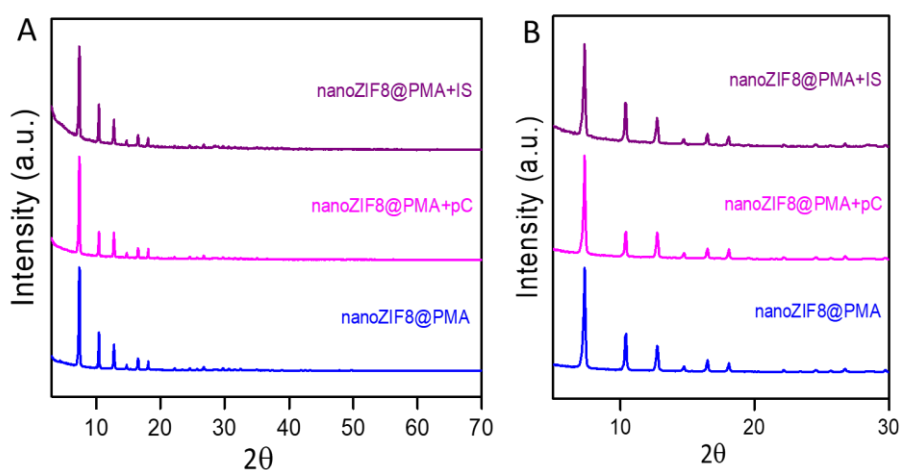


Fig. S8. PXRD patterns of @PMA particles as-prepared and after incubation with toxins solutions (0.3 mM pC or IS in PBS) for 24 h at 37 °C. (A) spectrum from 3° to 70° (2θ), and (B) magnification of the 2θ range between 3° and 30°.

III.5. Data comparison with other MOFs reported

Table S3 shows the comparative uptake of two related toxins, p-cresol (pC) or p-cresyl sulfate (pCS) by different MOFs; data of this work and those reported by Kato et al.⁶ and Cuchiari et al.⁷ These values correspond to raw data depicted in Figure 1G.

Table S3. Comparative uptake of pC or pCS reported by different MOFs

| MOF type | Toxin* | Uptake ($\mu\text{mol}\cdot\text{g}^{-1}$ MOF) | Conditions | Ref. |
|--------------|--------|---|--|-----------|
| nanoZIF8@PMA | pC | 131.2 | 24 h, 37 °C, PBS (pH=7.4) | This work |
| NU-1000 | pCS | 156.7 | 24 h, 24 °C, H ₂ O (pH≈6.5) | 6 |
| NU-901 | pCS | 131.7 | 24 h, 24 °C, H ₂ O (pH≈6.5) | 6 |
| NU-1010 | pCS | 48.3 | 24 h, 24 °C, H ₂ O (pH≈6.5) | 6 |
| NU-1200 | pCS | 10.5 | 24 h, 24 °C, H ₂ O (pH≈6.5) | 6 |
| MIL-100(Fe) | pCS | 68.6 | 24 h, 24 °C, H ₂ O (pH≈6.5) | 7 |
| MOF-808 | pCS | 23.6 | 24 h, 24 °C, H ₂ O (pH≈6.5) | 7 |
| MOF-808 | pCS | 10.3 | 24 h, 24 °C, H ₂ O (pH≈6.5) | 6 |
| UiO-67 | pCS | 7.8 | 24 h, 24 °C, H ₂ O (pH≈6.5) | 6 |
| UiO-NDC | pCS | 5.5 | 24 h, 24 °C, H ₂ O (pH≈6.5) | 6 |
| UiO-66 | pCS | 3.5 | 24 h, 24 °C, H ₂ O (pH≈6.5) | 6 |

IV. Immobilization of nanoZIF8@PMA within a rat kidney scaffold

PBS solutions prepared as described previously were autoclaved (30 min at 121 °C) and filtered through 0.2 µm filters in a laminar flow hood. Heparin (Sanofi, Gentilly, France) solution was prepared by dilution with sterile PBS at a concentration of 500 units per liter. Sodium dodecyl sulfate (SDS, Thermo Fisher Scientific #BP166-500) and Triton X-100 (ACROS Organics #215680010) solutions were made up in sterilized distilled water (dH₂O) at a concentration of 0.66 % and 1 %, respectively. Dissolution was assisted by heating, and all solutions were then filtered to remove small amounts of undissolved solute. Trisodium citrate buffer solution (0.2 M, pH=5.5) was prepared adding appropriate amounts of trisodium citrate (Merck #106448) to sterile PBS, adjusting pH and filtering through 0.2 µm filters in a laminar flow hood. All solutions were prepared under sterile conditions and were kept to 4 °C until used.

IV.1. Kidney decellularization protocol

Kidney organs were harvested from male 350-380 grams (g) Wistar rats. All experimental protocols were reviewed and approved by Ethics Committee for Animal Research of the University of Córdoba and by Junta de Andalucía (Ethical Code Number 17/07/2017/093). All rats received humane care in compliance with the guiding principles in the Guide for the Care and Use of Laboratory Animals. After anesthesia with isoflurane, a median laparotomy and systemic heparinization by injecting a single dose of heparin (2.0 units of heparin per g of body weight) through the infrahepatic inferior vena cava for anticoagulation was made. Left kidney, renal vein, renal artery and ureter were identified and isolated from surrounding fat. Subsequently, the whole kidney was harvested and transferred to a cell cultured dish. The whole kidney was maintained hydrated with cooled PBS while the main vasculature of the organ was cannulated.

The decellularization protocol was performed as previously described by Guerrero *et al.*⁸ Aseptic conditions were extremely important to avoid contamination during the decellularization process. Briefly, renal artery was cannulated with a 22-G cannula (Braun #4251628-01) and fixed with 3/0 silk suture. Kidney was manually perfused with 10 mL of diluted heparin solution to remove residual blood. Then, the cannulated kidney was mounted into the decellularization chamber and was connected to the peristaltic pump. The decellularization process was initiated by perfusion with diluted heparin solution for 30 min, followed by 0.66% SDS solution for 18 h until organ translucency was confirmed. Finally, the kidney was perfused with autoclaved dH₂O for 2 h and 1% Triton X-100 solution for 2 h. Perfusion rate for each step was set at 24 mL·h⁻¹. Following decellularization, we washed the kidney scaffold with PBS containing 10.000 U·mL⁻¹ penicillin G, 10 mg·mL⁻¹ streptomycin and 25 µg·mL⁻¹ amphotericin B (Sigma-Aldrich #A5955) at 18 mL·h⁻¹ constant arterial perfusion for 96 h. Wash solution was changed every 24 h.

IV.2. Perfusion of nanoparticles through a kidney scaffold

Kidney scaffold was manually perfused with 10 mL of citrate buffer and incubated at 37°C in an atmosphere of 5% CO₂ and 95% humidity for acclimatization. Before perfusion of nanoparticles, renal vein and ureter were clamped with an autoclaved stainless-steel micro serrefines (FST #18055). After that, 1 mL of the nanoZIF8@PMA particles dispersed in a buffer solution at a concentration of 10 mg·mL⁻¹ (amount optimized to achieve quantitative retention) was injected through the cannula into decellularized matrix. Cannula was closed with a cap and kidney

scaffold was placed in a petri dish in static culture overnight to ensure the binding of nanoZIF8@PMA particles to the extracellular matrix. Next day, the kidney scaffold was brought into a laminar flow hood, renal vein and ureter were unclamped (Fig. S9) and the kidney scaffold was manually perfused with PBS to remove potential unretained nanoparticles.

To determine the maximum amount of nanoZIF8@PMA particles that could be retained on the scaffold, we performed several experiments with fluorescent RhB-nanoZIF8@PMA to easily monitor the saturation point; no reddish color or red fluorescence detected in the wash solution indicated complete retention of the particles in the scaffold. Note that the size/weight between decellularized scaffolds varies slightly (for example, 1.285 g, 1.223 g, and 1.123 g for $n = 3$; average weight = 1.210 g), so to ensure the same number of particles in all of them, we decided to take an amount somewhat lower than the maximum derived from these experiments. This amount was set at 10 mg of particles per scaffold (perfusing 1 mL of particles at 10 mg·mL⁻¹). Assuming 1,210 g as the average weight of a decellularized scaffold, ZIF8 scaffolds have 8.3 mg of nanoZIF8@PMA per gram of scaffold.

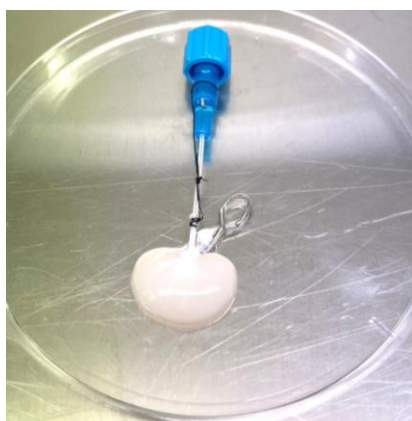


Fig. S9. Renal artery, vein and ureter clamped after manual perfusion of nanoZIF8@PMA particles through the decellularized kidney scaffold.

For microscopy analysis, kidney scaffold transverse sections were fixed in 4% paraformaldehyde and embedded in paraffin. Three-micrometer paraffin sections were obtained and examined using a Zeiss LSM 710 Confocal Laser Scanning Microscopy (Zeiss, Germany). Control experiments by perfusing free RhB dye solution and different types of particles (RhB-nanoZIF8, RhB-nanoZIF8@PMA, and RhB-nanoZIF8@PMA-FA) were performed under the same conditions, and different types of particles to investigate the role of the PMA and the stability of the particles under the scaffold microenvironment and during performance of the modified scaffold. Fig. S10 shows additional confocal images (in addition to those presented in the main manuscript) of the scaffold modified with the doubly fluorescent-labelled nanoZIF8@PMA particles.

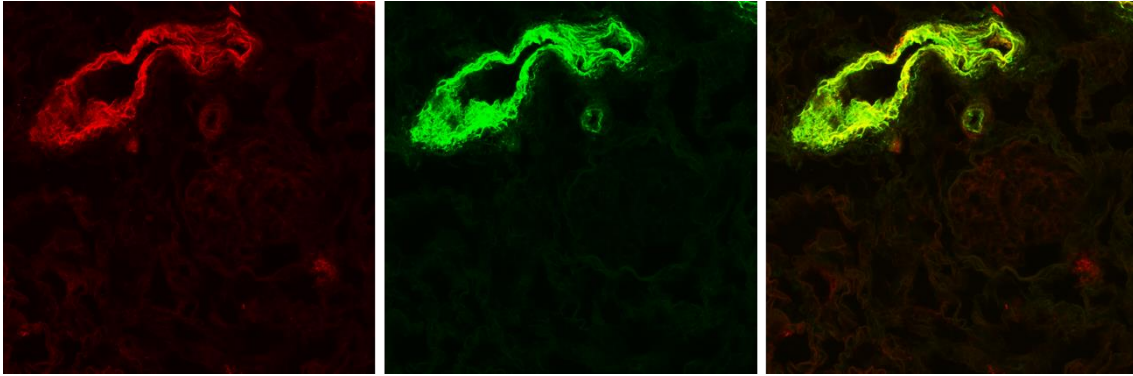


Fig. S10. Representative confocal microscopy images (40X magnification) of scaffolds modified with RhB-nanoZIF8@PMA-FA particles. Fluorescent channels correspond to: red channel for RhB ($\lambda_{\text{ex}}=514$ nm, $\lambda_{\text{em}}=575-650$ nm) and green channel for FA ($\lambda_{\text{ex}}=488$ nm, $\lambda_{\text{em}}=500-575$ nm).

V. Performance evaluation of nanoZIF8-modified scaffold

V.1. Procedure of adsorption experiments under flow conditions

Solutions of uremic toxins (pC and IS at 0.3 mM in PBS) were freshly prepared (as described above) before use. To carry out these experiments nanoZIF8@PMA particles were injected within kidney scaffold as described above to have the nanoZIF8-modified scaffold (ZIF8-scaffold). For each experiment, a control kidney scaffold and a ZIF8-scaffold were attached to a bioreactor and perfused with 10 mL of IS or pC solution for 24 h at 12 mL·h⁻¹ flow rate in an incubator at 37°C in an atmosphere of 5% CO₂ and 95% humidity using a closed system bioreactor. After this time, the perfused solutions were collected and quantitatively analyzed by reversed-phase high-performance liquid chromatography with diode array detection (RP-HPLC-DAD). Three independent experiments were conducted for each condition.

V.2. Quantification of toxins by RP-HPLC-DAD

The RP-HPLC-DAD analyses were carried out on a Shimadzu Prominence-i LC-2030C 3D chromatograph equipped with a deuterium UV diode array detector (DAD), a column oven, and an autosampler (Shimadzu, Kyoto, Japan). Analyses were performed using a C18 column (3 μm, 50 mm × 4.6 mm, pore size 100 Å; Phenomenex #00B-4251-E0) and the solvent used as mobile phase (under isocratic conditions) was acetonitrile: 0.01 M ammonium acetate (pH 5) = 20:80 (v/v). The flow rate was 1 mL·min⁻¹, the column temperature was kept at 35 °C, 20 μL of standard or sample solution was injected, and the total analysis time was 10 min. The wavelengths of detection (at the maximum absorption peak) were 221 nm for pC and 219 nm for IS. Calibration curves were constructed by plotting peak area against the corresponding concentration (mM) of each standard (Fig. S11).

To determine the toxin concentration in the collected samples of perfusate after passing through the scaffold (that is, the non-adsorbed fraction), these samples were analyzed by HPLC-DAD using the described method and concentrations were calculated by interpolation into the calibration curves. Then, based on the difference between the initial concentration and the non-adsorbed fraction, the fraction that was adsorbed on the ZIF8-scaffold was calculated. The removal efficiency was calculated by using the Equation 1 indicated above.

In the case of the analyses of the toxins in human serum the RP-HPLC-DAD method was slightly modified to achieve an appropriate chromatographic separation of the toxins from the serum constituents. Specifically, we changed the column (XSelect HSS C18, 3.5 μm, 150 mm × 4.6 mm, pore size 100 Å; Waters #186004768) and the analysis time (30 min). Representative chromatograms of the analyses of human serum fortified with the toxins (0.3 mM each one) before and after perfusion through the ZIF8-modified scaffold are shown in Fig. S12.

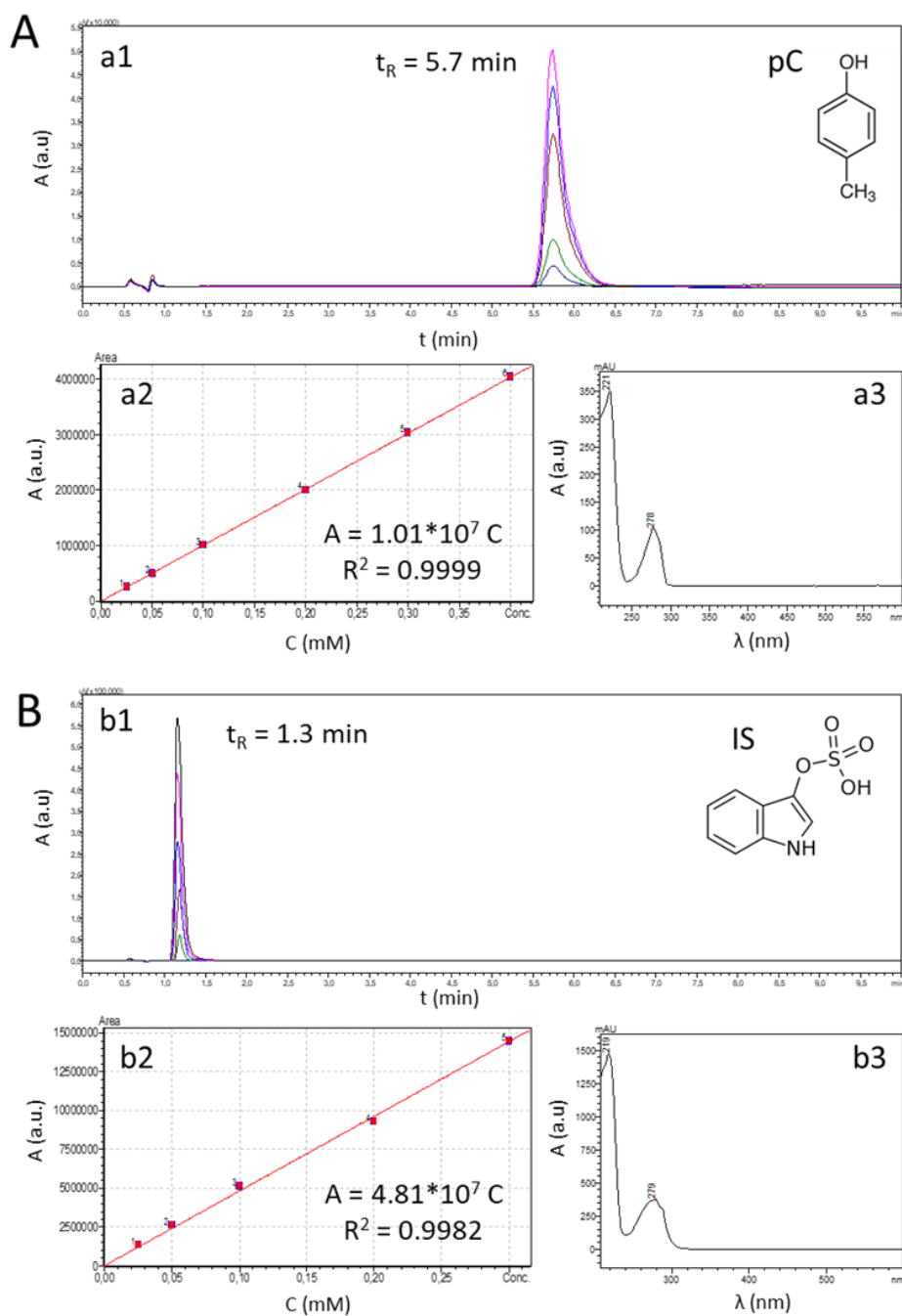


Fig. S11. (A) Calibration data for pC: (a1) RP-HPLC-DAD chromatograms obtained for the different pC standards; (a2) calibration curve constructed by plotting the integrated absorbance peak as a function of pC concentration; (a3) representative the UV-Vis absorbance spectrum of pC. (B) Calibration data for IS: (b1) RP-HPLC-DAD chromatograms obtained for the different IS standards; (b2) calibration curve constructed by plotting the integrated absorbance peak as a function of IS concentration; (b3) representative the UV-Vis absorbance spectrum of IS. Calibration equations are obtained by fitting a linear regression line to the collected data (a2 and b2); R^2 is the coefficient of determination.

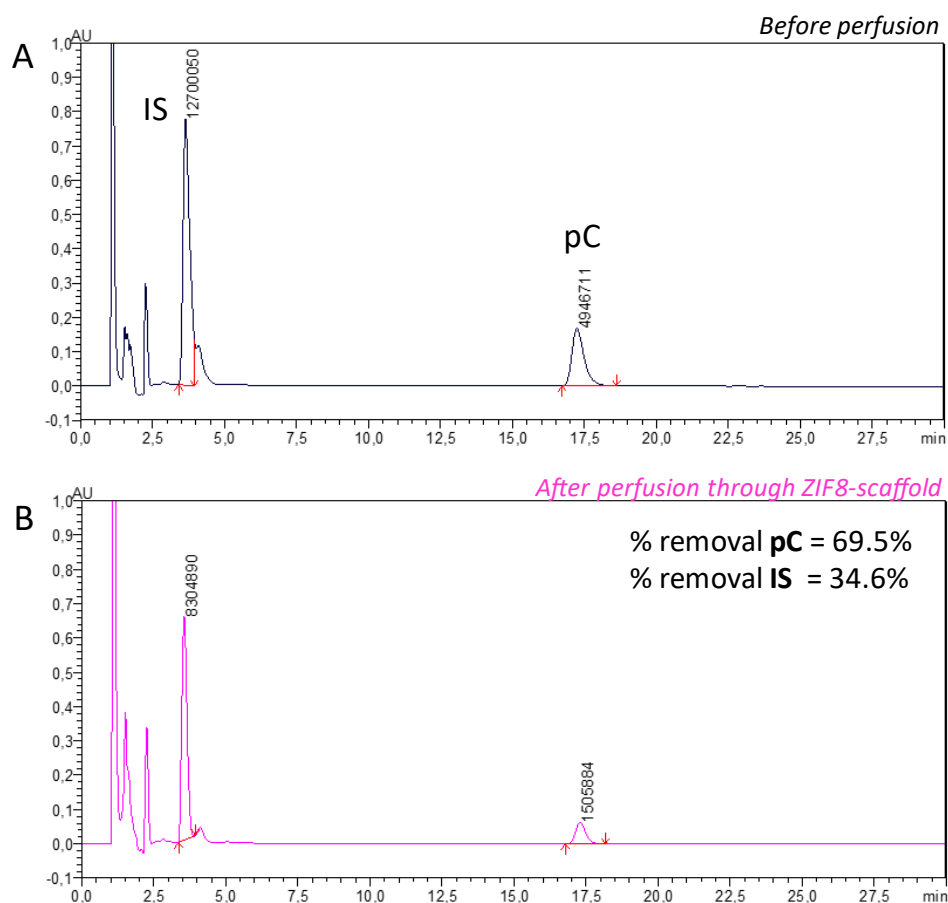


Fig. S12. RP-HPLC-DAD chromatograms obtained for the analyses of human serum containing pC and IS (0.3 mM) before (A) and after being perfused through the ZIF8-scaffold (B).

V.3. Evaluation of the reusability of nanoZIF8-modified scaffold

Studies focused to assess the reusability of the ZIF8-scaffolds were performed. After each use, the ZIF8-scaffold was washed with PBS and fresh uremic toxin solution, pC or IS, were again perfused for 24 h at $12 \text{ mL}\cdot\text{h}^{-1}$ flow rate in an incubator at $37 \text{ }^\circ\text{C}$ in an atmosphere of 5% CO_2 and 95% humidity using a closed system bioreactor. ZIF8-scaffolds were reused three times. The perfusate obtained of each use was collected and quantitatively analyzed by RP-HPLC-DAD as previously described. Data are shown in Fig. 3E. A similar reuse experiment was carried out with a scaffold modified with fluorescent-labelled nanoZIF8@PMA particles. Comparing the confocal images of the ZIF8-scaffold after three uses (i.e., after perfusion of toxins for 3 sequential cycles) with those obtained before use (Fig. S13), it seems clear that the particles remained at the same location within the extracellular matrix.

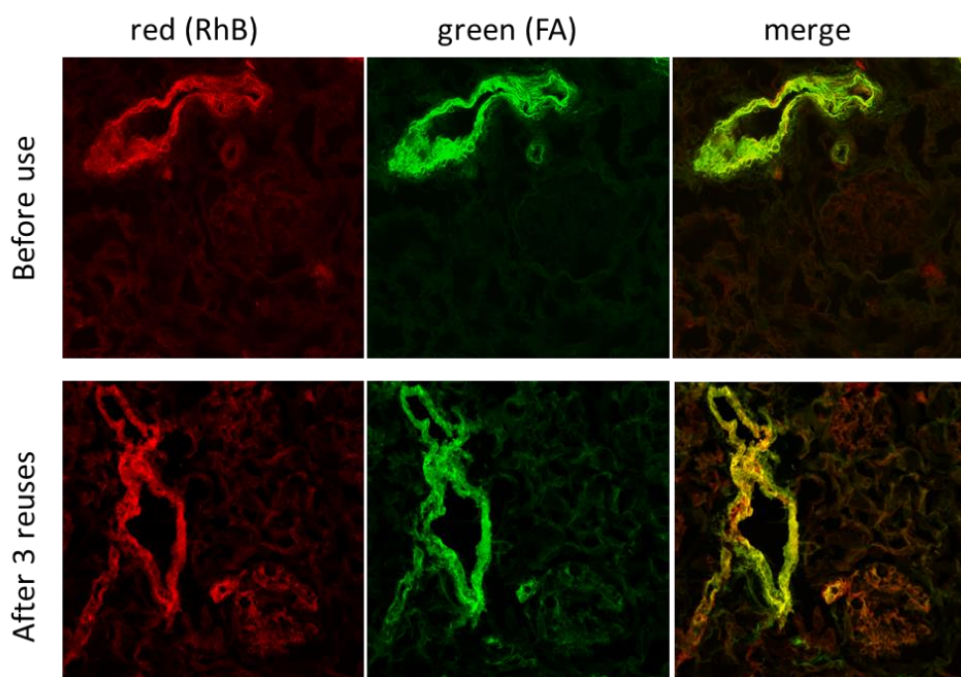


Fig. S13. Representative confocal microscopy images (40X magnification) of scaffolds modified with RhB-nanoZIF8@PMA-FA particles (A) before use and (B) after three reuses. Fluorescent channels correspond to: red channel for RhB ($\lambda_{ex}=514$ nm, $\lambda_{em}=575-650$ nm) and green channel for FA ($\lambda_{ex}=488$ nm, $\lambda_{em}=500-575$ nm).

V.4. Statistical analysis

Quantitative variables were expressed as means \pm standard deviation. Data distribution was analyzed with the Shapiro-Wilk test to verify a normal distribution. The difference between means for two different groups was assessed by Student's t test. The difference between means for three groups was determined by ANOVA with Bonferroni post hoc correction. Values of p lower than 0.05 were considered to be significant. Data were analyzed using SPSS Statistics software version 25.0 (SPSS, Inc., Chicago, IL, USA).

VI. Performance evaluation of nanoZIF8-modified scaffold

VI.1. Computational details

The adsorption of uremic toxins pC and IS, as well as phosphate, was studied using the molecular simulation software RASPA.⁹ The geometry of ZIF-8 was initially optimised with the quantum mechanical simulation software package¹⁰ DFTB+, which allows the simulation of periodic systems. The Tight-Binding GFN2-xTB method¹¹ was used in the geometry optimisation, and the Mulliken charges of the framework atoms were also calculated.

The calculation of the atomic charges of the guest molecules (pC, IS, and sodium phosphate) was performed with the computational chemistry software package Gaussian 09.¹² The molecules were initially optimised using the hybrid exchange-correlation functional wB97X,¹³ and the large 6-311++G(d,p) triple- ζ basis set with polarization and diffuse functions, in order to reduce basis set superposition errors. After the optimisation, the atomic charges were calculated using CHELPG (CHarges from Electrostatic Potentials using a Grid-based method).¹⁴ Fig. S14 shows the two toxin molecules studied, pC and IS.

The Lennard-Jones parameters were taken from the Universal Force Field, UFF.¹⁵ Host-guest and guest-guest interactions were described using Lorentz-Berthelot mixing rules. Electrostatic interactions are calculated using the Ewald summation method.¹⁶

The adsorption of the guest molecules was studied using Grand Canonical Monte Carlo (GCMC) simulations, performed with the RASPA code.⁹ We carried out 10^2 initialisation cycles, followed by 10^4 equilibration cycles, and finally $2 \cdot 10^5$ production cycles. The temperature of the calculations was 37 °C, which is the temperature of the human body, at which the experiments were performed. The pressure was set to 75 Pa, which corresponds to the concentrations of 0.3 mM employed in the adsorption experiments with nanoZIF8@PMA particles.

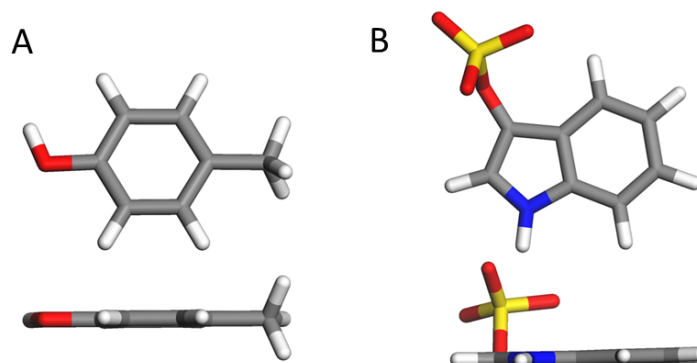


Fig. S14. Top and side views of the optimised geometries of the (A) pC and (B) IS molecules. Color code: H, white; C, grey; N, blue; O, red; S, yellow.

VI.2. Adsorption of pC and IS, pure and mixed with phosphate molecules

The GCMC simulations of the pC and IS molecules, when modelled in pure phases, were high in comparison with experiments. The calculated loadings were $3661 \mu\text{mol}\cdot\text{g}^{-1}$ and $1830 \mu\text{mol}\cdot\text{g}^{-1}$, respectively, much higher than the experimental values for pC and pC adsorption, of $99 \mu\text{mol}\cdot\text{g}^{-1}$ and $131 \mu\text{mol}\cdot\text{g}^{-1}$, respectively. Fig S15 (also shown in the main text as Fig. 1H) shows the geometries of the adsorbed molecules.

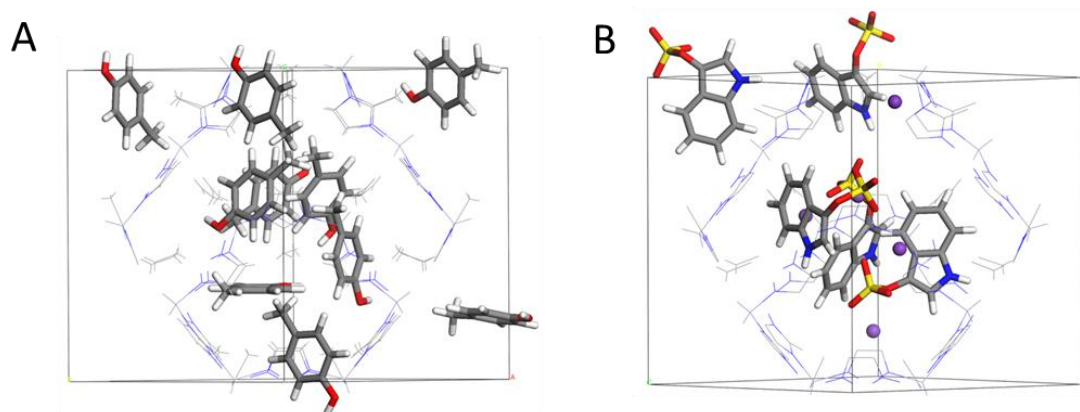


Fig. S15. View of the ZIF-8 structure in which pC (A) and IS (B) molecules have been adsorbed, using GCMC simulations. Colour code: H=white; C=grey; N =blue; O=red; S=yellow; K=violet. H atoms of the framework structure have been omitted for clarity reasons.

The theoretical loadings of pC ($3661 \mu\text{mol}\cdot\text{g}^{-1}$) and IS ($1830 \mu\text{mol}\cdot\text{g}^{-1}$) are the highest theoretical loadings that the ZIF-8 system would be able to adsorb, when a phase of pure molecules is adsorbed. We must note that pC has a higher maximum theoretical loading than IS, in accordance with its smaller size (static kinetic diameters of 4.28 \AA for pC and 5.01 \AA for IS), which permits a better packing of molecules, as observed in Fig. S15. Another factor inducing the higher adsorption of pC with respect to IS is the fact that IS molecules cannot be adsorbed into the ZIF-8 structure by themselves, since they are charged species, and the introduction of charged species would create an electric field which would rapidly preclude the adsorption of more charged species. Instead, they are accompanied by their counterions, which are K^+ cations. These cations must also fit inside the ZIF-8 pores, thus reducing the number of IS molecules that can be adsorbed.

We must also note that both pC and IS molecules are larger than the theoretical limiting window size of ZIF-8, 3.4 \AA , as estimated from XRD data. But it is known that molecules larger than this size can diffuse through ZIF-8, thanks to the flexibility of the framework,¹⁸ which allows the diffusion of benzene molecules, for instance.¹⁹ Nevertheless, the bulkier nature of IS will induce a slower diffusion than that of pC, as observed experimentally. In Fig. S16 (also shown in the main text as Fig. 1G) we can clearly see why pC diffusion would be faster than IS, by observing the larger distortion needed for the ZIF-8 window to permit the flow of IS molecules.

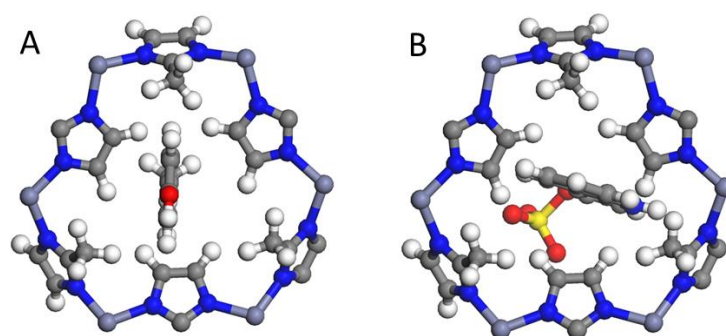


Fig. S16. View of a 6-member ring window of the ZIF-8 structure, through which pC (A) and IS (B) molecules must pass to diffuse within the framework. Colour code: H=white; C=grey; N =blue; O=red; S=yellow.

The large difference between the theoretical and experimental values of toxins loadings is likely due to the difference between our model and the real solutions. Indeed, it is remarkable that a model as simple as ours can predict loadings that are around an order of magnitude from the experimental values. We therefore aimed to obtain more accurate results, by increasing the complexity of our model. For that reason, we included another species, phosphate ions, which can be adsorbed with the uremic toxins. The PBS buffer solution in which the uremic toxins are immersed has a 0.137 M concentration of NaCl and 0.01 M concentration of sodium phosphate, plus other, less concentrated species. In order to carry out a very accurate study, with which to obtain theoretical loadings in quantitative agreement with experiment, we would need to perform interatomic potential fittings to improve the description of the interactions, both in terms of the UFF Lennard-Jones potentials and in terms of the intramolecular force field, although it would require a very long time. We will therefore include the effect of sodium phosphate species in PBS, for which the interatomic potential is likely to perform better than for NaCl. When the adsorption of sodium phosphate/uremic toxins mixtures is studied, there is a clear competition between the two species, thus lowering the amount of toxins that can be adsorbed. The theoretical loadings get reduced from $1830 \mu\text{mol}\cdot\text{g}^{-1}$ to $732 \mu\text{mol}\cdot\text{g}^{-1}$ for IS, and from $3661 \mu\text{mol}\cdot\text{g}^{-1}$ to $1098 \mu\text{mol}\cdot\text{g}^{-1}$ for pC. We see a big decrease in the adsorption of toxin molecules, due to the competition with sodium phosphate. Fig. S17 shows the two mixtures of species adsorbed after the GCMC simulations.

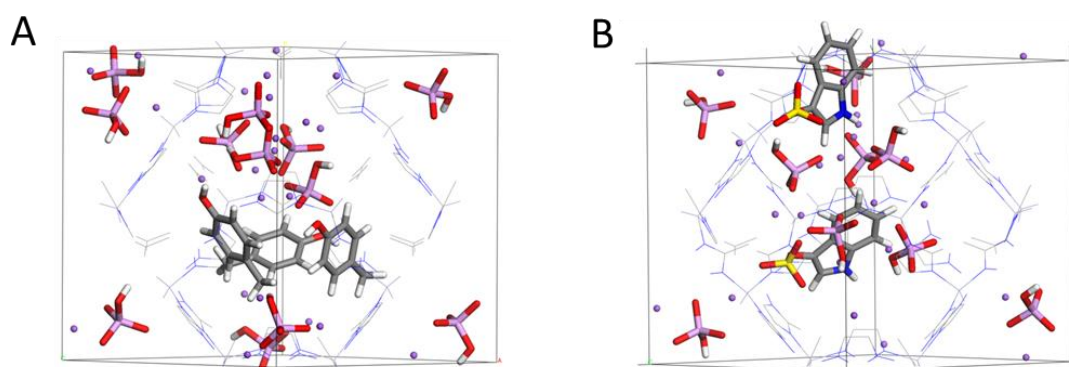


Fig. S17. View of the ZIF-8 structure in which pC (A) and IS (B) molecules have been loaded, together with sodium phosphate, using GCMC simulations. Colour code: H=white; C=grey; N=blue; O=red; S=yellow; K=violet; P=pink. H atoms of the framework structure have been omitted for clarity reasons.

The decrease in theoretical loadings upon the increase in the complexity of the model confirms our initial hypothesis, i.e., that the discrepancy between the calculated and experimental values arises from the inaccurate nature of our model. As mentioned above, it is therefore likely that a quantitative agreement would be achieved, but it falls out of the scope of this study. Our calculations have shown that the values of loadings observed experimentally are in the expected range for adsorption within the ZIF-8 pores, so we can state that uremic molecules are indeed adsorbed in the nanoZIF8@PMA structures, not on their surfaces.

VII. References

1. J. Hühn, C. Carrillo-Carrion, M. G. Soliman, C. Yue, M. Carril, N. Feliu, A. Escudero, A. M. Alkilany, B. Pelaz, P. del Pino and W. J. Parak, *Chem. Mater.* 2017, **29**, 399.
2. C. Carrillo-Carrión, R. Martínez, M. F. Navarro Poupard, B. Pelaz, E. Polo, A. Arenas-Vivo, A. Olgiati, P. Taboada, M. G. Soliman, U. Catalán, Fernández-Castillejo, R. Solà, W. J. Parak, P. Horcajada, R. A. Alvarez-Puebla and P. del Pino, *Angew. Chem. Int. Ed.* 2019, **58**, 7078.
3. M. Menendez-Miranda, J. M. Costa-Fernández, J. R. Encinar, W. J. Parak and C. Carrillo-Carrion, *Analyst* 2016, **141**, 1266.
4. C. Carrillo-Carrion, A. I. Bocanegra, B. Arnaiz, N. Feliu, D. Zhu and W. J. Parak, *ACS Nano* 2019, **13**, 4631.
5. Cohen, P.P. De Deyn, R. Deppisch, B. Descamps-Latscha, T. Henle, A. Jörres, H. D. Lemke, Z. A. Massy, J. Passlick-Deetjen, M. Rodriguez, B. Stegmayr, P. Stenvinkel, C. Tetta, C. Wanner and W. Zidek, *Kidney Int.* 2003, **63**, 1934.
6. S. Kato, K. Otake, H. Chen, I. Akpinar, C. T. Buru, T. Islamoglu, R. Q. Snurr and O. K. Farha, *J. Am. Chem. Soc.* 2019, **141**, 2568.
7. H. Cuchiaro, J. Thai, N. Schaffner, R. R. Tuttle and M. Reynolds, *ACS Appl. Mater. Interfaces* 2020, **12**, 22572.
8. F. Guerrero, A. Carmona, R. Ortega, S. Cañadillas, R. Crespo, C. Herrera and P. Aljama, *JBISE*. 2017, **10**, 509.
9. D. Dubbeldam, S. Calero, D. E. Ellis and Randall Q. Snurr, *Molecular Simulation*, 2016, **42**, 81.
10. B. Hourahine, B. Aradi, V. Blum, F. Bonafé, A. Buccheri, C. Camacho, C. Cevallos, M. Y. Deshayé, T. Dumitrică, A. Dominguez, S. Ehlert, M. Elstner, T. van der Heide, J. Hermann, S. Irle, J. J. Kranz, C. Köhler, T. Kowalczyk, T. Kubař, I. S. Lee, V. Lutsker, R. J. Maurer, S. K. Min, I. Mitchell, C. Negre, T. A. Niehaus, A. M. N. Niklasson, A. J. Page, A. Pecchia, G. Penazzi, M. P. Persson, J. Řezáč, C. G. Sánchez, M. Sternberg, M. Stöhr, F. Stuckenberg, A. Tkatchenko, V. W.-z. Yu, and T. Frauenheim, *J. Chem. Phys.* 2020, **152**, 124101.
11. C. Bannwarth, S. Ehlert and S Grimme, 2019, *J. Chem. Theory Comput.*, **15**, 1652.
12. M. J. Frisch, G. W. Trucks, H. B. Schlegel, G. E. Scuseria, M. A. Robb, J. R. Cheeseman, G. Scalmani, V. Barone, B. Mennucci, G. A. Petersson, H. Nakatsuji, M. Caricato, X. Li, H. P. Hratchian, A. F. Izmaylov, J. Bloino, G. Zheng, J. L. Sonnenberg, M. Hada, M. Ehara, K. Toyota, R. Fukuda, J. Hasegawa, M. Ishida, T. Nakajima, Y. Honda, O. Kitao, H. Nakai, T. Vreven, J. A. Montgomery, Jr., J. E. Peralta, F. Ogliaro, M. Bearpark, J. J. Heyd, E. Brothers, K. N. Kudin, V. N. Staroverov, R. Kobayashi, J. Normand, K. Raghavachari, A. Rendell, J. C. Burant, S. S. Iyengar, J. Tomasi, M. Cossi, N. Rega, J. M. Millam, M. Klene, J. E. Knox, J. B. Cross, V. Bakken, C. Adamo, J. Jaramillo, R. Gomperts, R. E. Stratmann, O. Yazyev, A. J. Austin, R. Cammi, C. Pomelli, J. W. Ochterski, R. L. Martin, K. Morokuma, V. G. Zakrzewski, G. A. Voth, P. Salvador, J. J. Dannenberg, S. Dapprich, A. D. Daniels, Ö. Farkas, J. B. Foresman, J. V. Ortiz, J. Cioslowski, and D. J. Fox, Gaussian 09 (Gaussian, Inc., Wallingford CT, 2009).
13. C. Jeng-Da, and H.-G. Martin, *J. Chem. Phys.* 2008, **128**, 084106.

14. C.M. Breneman, K.B.J. Wiberg *J. Comput. Chem.*, 1990, **11**, 361.
15. Stephen L. Mayo, Barry D. Olafson, and William A. Goddard, *J. Phys. Chem.* 1990, **94**, 8897.
16. T. Darden, D. York, and L. Pedersen, 1993, *J. Chem. Phys.* **98**, 10089.
17. T. Chokbunpiam, R. Chanajaree, O. Saengsawang, S. Reimann, C. Chmelik, S. Fritzsche, J. Caro, T. Remsungnen, S. Hannongbua, 2013, *Microporous Mesoporous Mater.* **174**, 126.
18. F-X Coudert, 2017, *ChemPhysChem*, **18**, 2732.
19. L. Diestel, H. Bux, D. Wachsmuth, J. Caro, 2012, *Micropor. Mesopor. Mater.* **164**, 288.